



REGIONALIZATION OF PRECIPITATION, ITS AGGRESSIVENESS AND CONCENTRATION IN THE GUAYAS RIVER BASIN, ECUADOR

REGIONALIZACIÓN DE LA PRECIPITACIÓN, SU AGRESIVIDAD Y CONCENTRACIÓN EN LA CUENCA DEL RÍO GUAYAS, ECUADOR

Mercy Ilbay-Yupa*¹ , Ricardo Zubieta Barragán²  and Waldo
Lavado-Casimiro³ 

¹ Facultad de Ciencias Agropecuarias y Recursos Naturales, Universidad Técnica de Cotopaxi, Av Simón Rodríguez, Latacunga, Ecuador

² Departamento de Ciencias de la Atmósfera e Hidrósfera, Instituto Geofísico del Perú, Av. Badajoz 169, Ate 15012, Lima, Perú

³ Programa de Doctorado en Recursos Hídricos, Universidad Nacional Agraria La Molina, La Molina 15024 Lima, Perú

*Corresponding author: mercy.ilbay@utc.edu.ec

Article received on June 6th, 2019. Accepted, after review, on August 12th, 2019. Published on September 1st, 2019.

Resumen

La agresividad de la lluvia contribuye a la erosividad del suelo en regiones de alta montaña, y por ende a la sedimentación en la parte baja de la cuenca. El conocimiento acerca de la agresividad de la lluvia en regiones costeras y andinas contribuye a la formulación de medidas de mitigación que influyen en la reducción de erosión y pérdida de nutrientes. Los índices Fournier, Fournier modificado y de concentración de precipitación proveen la capacidad de estimar la distribución espacial y temporal de la agresividad de la lluvia. Este estudio presenta un análisis de la lluvia mediante estos índices de agresividad en la cuenca del río Guayas ubicada en la costa y Andes ecuatoriales. Se seleccionaron datos mensuales registrados de 30 estaciones pluviométricas para el período 1968-2014. Se determinaron zonas homogéneas de precipitación mediante el método k-means. Los resultados indicaron dos regiones homogéneas predominantes, la primera ubicada al oeste en la zona costera y andina (85,2% del área de la cuenca), con un índice de agresividad alto y muy alto; mientras que la distribución de la precipitación en la segunda región (Alta montaña) resultó de muy baja a baja agresividad. La mayor agresividad potencial de la lluvia le corresponde una mayor acumulación de precipitación promedio anual, lo que indica una alta influencia estacional de las lluvias, es decir, una mayor cantidad de lluvia puede precipitar en un número reducido de meses consecutivos. Los valores de concentración revelan un gradiente regional en dirección este-oeste que va de moderadamente a fuertemente estacional. El análisis de tendencias de la concentración de lluvia mensual no muestra cambios significativos en el período de estudio. No obstante, los hallazgos del presente estudio explican el porqué la región oeste y sur de la cuenca del río Guayas está expuesta a problemas de sedimentación en la parte baja, producto de la capacidad erosiva de la lluvia en la parte alta y media de la cuenca.

Palabras clave: Guayas, concentración, precipitación, agresividad, erosividad, Ecuador.

Abstract

The aggressiveness of rain contributes to the erosion of the soil in high mountain regions, and therefore to the sedimentation in the lower part of the watershed. To know about the aggressiveness of rain in coastal and Andean regions contributes to the formulation of mitigation measures that help to the reduction of erosion and loss of nutrients. Fournier indices, Modified Fournier and precipitation concentration provide the ability to estimate the spatial and temporal distribution of the aggressiveness of the rain. This study presents a spatial and temporal analysis of climatic aggressiveness in the Guayas river watershed located on the coast and the equatorial Andes. Registered monthly data of 30 rainfall stations for the period 1968-2014 was selected. Homogeneous precipitation zones were determined by the k-means method. The results indicated two predominant homogenous regions, the first located to the west in the coastal and Andean zone (85,2% of the area of the Watershed), with a high and very high aggressiveness index, while the distribution of precipitation in the second region (High mountain) resulted from very low to low aggressiveness. The greater potential aggressiveness of rain corresponds to a greater accumulation of average annual rainfall, which indicates a high seasonal influence of rainfall, i.e., a greater amount of rainfall can precipitate in a reduced number of consecutive months. The concentration values reveal a regional gradient in the east-west direction, which goes from moderately to strongly seasonal. The trend analysis of the monthly rainfall concentration shows no significant changes in the study period. However, these findings explain why the western and southern region of the Guayas river watershed is exposed to sedimentation problems in the lower part, due to the erosive capacity of rain in the higher and middle part of the watershed.

Keywords: Guayas, concentration, precipitation, aggressiveness, erosivity, Ecuador.

Suggested citation: Ilbay-Yupa, M., Zubieta B., R. and Lavado-Casimiro, W. (2019). Regionalization of precipitation, its aggressiveness and concentration in the Guayas river basin, Ecuador. *La Granja: Revista de Ciencias de la Vida*. Vol. 30(2):52-69. <http://doi.org/10.17163/lgr.n30.2019.06>.

Orcid ID:

Mercy Ilbay-Yupa: <http://orcid.org/0000-0001-9503-2686>

Ricardo Zubieta Barragán: <https://orcid.org/0000-0002-4315-7695>

Waldo Lavado-Casimiro: <https://orcid.org/0000-0002-0051-0743>

1 Introduction

The erosion of precipitation causes loss of fertile soil, damage to infrastructure, agriculture and water pollution, which is influenced by changes in precipitation patterns (Martín-Fernández and Martínez-Núñez, 2011; Sanchez-Moreno et al., 2014). This is caused since large amounts of seasonal rain can precipitate in high mountain regions such as the Andes in a few days or weeks (Sarricolea et al., 2014; Zubieta et al., 2016; Sarricolea et al., 2019), or Amazonian regions (Zubieta et al., 2019). Precipitation is an important variable for climate studies, whose spatial and temporal variability can impact human activities during extreme hydroclimatic events such as droughts and floods (Parracho et al., 2016). It also plays a key role in water resource planning and management, directly linked to agriculture and disaster mitigation (Prakash et al., 2015). Accurate precipitation quantification is a challenge for many hydrological applications, especially in regions with complex topography due to orographic and small-scale slope effects (Prakash et al., 2015)

The aggressiveness of rain can cause environmental impacts and is a key factor in the occurrence of soil erosion, landslides or flooding. Therefore, parameters that evaluate the aggressiveness of rain can be considered as an appropriate environmental indicator ((Gregori et al., 2006; García-Barrón et al., 2018). Estimating this variable over long periods is useful for the soil conservation, agricultural planning and environmental policy development. The R-factor, or rainfall erosivity, is an accepted instrument for measuring local erosion and it depends on the kinetic energy of each rain episode ((Panagos et al., 2015). This model is the most widely used and was developed on a detailed scale in the agricultural sector; however, its application at the regional level presents limitations (Terranova et al., 2009). The soil erosion estimates do not conform to empirical sedimentation measures and do not incorporate direct water runoff (Kinnell, 2010).

The R-factor overestimates erosion at the regional or watershed level (Hernando and Romana, 2016) and is not recommended in areas where a validation process is not performed. In addition, it is advisable to use high-frequency precipitation records of weather stations for a period of more than twenty years for its estimation (Angulo-Martínez et al., 2009). Therefore, models that measure the effects of rainfall aggressiveness can be used by considering hourly rainfall records (intensity models) or monthly precipitation records (volume models). The latter model refers to the different partial accumulations

of rain, regardless of the number, duration and amount of rain of each episode, so it is based exclusively on monthly precipitation records available in most countries. Thus, the aggressiveness index can be used in environmental studies (Fournier, 1960; Arnoldus, 1978; Oliver, 1980). These indices have been widely used in climate studies to identify spatial rainfall concentration patterns in regions of Europe, Asia, Africa and South America such as Spain (De Luis et al., 2011), Iberian Peninsula (García-Barrón et al., 2018), India (Ballari et al., 2018), Bangladesh (Rasel et al., 2016), Nigeria (Ezenwaji et al., 2017), Argentina (Besteiro and Delgado, 2011), Venezuela (Rey et al., 2012) and Chile (Sarricolea et al., 2014; Valdés-Pineda et al., 2016). Changes in the temporal patterns of these parameters have also been identified in Andean regions of Chile (Sarricolea et al., 2019).

The intense soil erosion resulting from increased rainfall intensity is a critical problem in many basins around the world (Vrieling et al., 2014; Mondal et al., 2016). The Guayas River Basin (CRG - acronym in Spanish), is Ecuador's most fertile agricultural area (Buckalew et al., 1998), and the main production center for agricultural goods. Seasonal distribution and annual rainfall totals are extremely irregular, causing CRG to be affected by flood events and droughts, causing economic losses. This was the case for 1982 and 1983, which produced estimated losses of 3,18% and 28,63% of PIB, respectively (\$520 million) (Egas, 1985). While in 1997-98 5664 km² of agricultural production (\$616,5 million) was lost (Corporación Andina de Fomento, 1998), caused by the marked influence of El Niño phenomenon on the basin (Cadier et al., 1996). But the area of greatest affectation is the low basin, because it is periodically subjected to flooding that can have catastrophic consequences, aggravated by human actions such as deforestation and erosion in the headwaters of the rivers (Rossel et al., 1996). The Guayas River presents sedimentation problems due to soil erosion in the basin (Gobierno Provincial del Guayas, 2016), which has resulted in the formation of islets at the junction of the Babahoyo and Daule River (Figure 1) (Soledispa, 2002). Measures such as dredging have been used in the face of sediment accumulation amounting to 250 thousand tons per year (Gobierno Provincial del Guayas, 2018). However, rain has not been studied as an erosion factor in Ecuadorian regions such as the CRG. The aim of this research is (a) to regionalize precipitation for a prolonged period of monthly precipitation data (1968-2014) and (b) to estimate the aggressiveness and concentration of precipitation in the CRG.

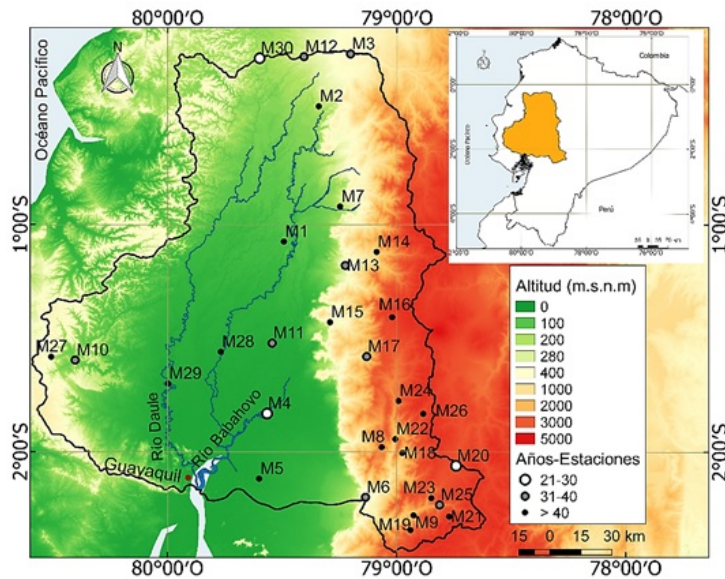


Figure 1. Location of the Guayas River basin, altitude, distribution of the 30 rainfall stations and years of study. The name of the stations is shown in Table 1.

2 Materials and methods

2.1 Study area

The CRG is located in the central western of Ecuador ($0^{\circ}14'$ a $2^{\circ}27'$ S y $78^{\circ}36'$ a $80^{\circ}36'$ O) (Figure 1). The area is characterized by a significant altitude gradient up to 4000 masl with an area of 32890km^2 , corresponding to 13% of Ecuador area. It concentrates approx 40% of the country's population (?). CRG drains into the Gulf of Guayaquil, the main rivers are the Daule and Babahoyo (Figure 1) that join near Guayaquil, the country's largest city Damanik-Ambarita2016. The Guayas River, the largest on the western coast of South America, with an average annual run of $1350\text{m}^3/\text{s}$ (Twilley et al., 2001), has a straight main channel forking into a network of river channels that run through 30 km of mangroves and tidal plains (Reynaud et al., 2018). The main economic activities in the CRG are: agriculture, fishing and hydroelectric power generation. The main environmental pressures on freshwater ecosystems are wastewater pollution, agriculture, land use changes and two hydroelectric dams (Thi Nguyen et al., 2015). In recent years, river sedimenta-

tion problems have increased in the lower part of the basin, considered to be one of the contributing factors to the risk of flooding from extreme rains. This sedimentation is perceived locally as a consequence of interventions carried out in the upper basin and natural events such as El Niño (Barrera-Crespo et al., 2018). The impacts of El Niño on this basin have caused flooding (rain erosion, slippage and landslides), pollution of drinking water, damage to infrastructure and the agricultural sector (Corporación Andina de Fomento, 1998).

2.2 Data

Precipitation records were collected from 250 weather stations from the National Institute of Meteorology and Hydrology (INAMHI), each with different periods between 1962 and 2016. In order to guarantee the highest availability of monthly data, 30 stations with a period of 47 years (1968-2014) were selected, which had the lowest amount (< 13%) of missing data (Table 1). Out of the 30 stations, 63% of them have more than 40 years of continuous records, and 10% from 21 to 30 years.

2.3 Methodology

The methodology consists of three summarized steps in Figure 2: the first is the evaluation of the precipitation data, its homogenization and the completion of monthly data by the regional vector (MVR) method. The second

corresponds to the process of regionalization by grouping stations using k-means and interpolation using co-kriging, and the last stage corresponds to the determination of the aggressiveness and concentration of precipitation through different indices.

Table 1. Characteristics of 30 stations in the Guayas River basin: name, geographical location and missing data.

Code	Name	Latitude (°S)	Length (°O)	Altitude (msnm)	% missing data	Period
M1	Pichilingue	-1.07	-79.49	81	0	1968-2014
M2	Puerto Ila	-0.48	-79.34	319	2	1968-2014
M3	Sto. Domingo Aeropuerto	-0.25	-79.20	554	6	1968-1998
M4	Isabel María	-1.83	-79.56	4	8	1968-1988
M5	Milagro (Ingenio Valdez)	-2.12	-79.60	23	0.2	1968-2014
M6	Bucay	-2.20	-79.13	480	4	1969-2000
M6	San Juan La Mana	-0.92	-79.25	215	9	1968-2014
M8	Chillanes	-1.98	-79.06	2330	4	1968-2014
M9	Chunchi	-2.28	-78.92	2177	3	1968-2014
M10	Camposano #2	-1.59	-80.40	113	1	1977-2014
M11	Pueblo Viejo	-1.52	-79.54	19	13	1976-2014
M12	Las Delicias-Pichincha	-0.26	-79.40	340	8	1968-2002
M13	Moraspungo-Cotopaxi	-1.18	-79.22	409	8	1968-87; 96-2014
M14	Ramón Campaña	-1.12	-79.09	1462	7	1968-2014
M15	Echeandia	-1.43	-79.29	308	9	1968-2014
M16	Salinas-Bolívar	-1.40	-79.02	3600	10	1969-2014
M17	Río San Antonio-Monjas	-1.58	-79.13	2200	2	1980-2014
M18	Pallatanga	-2.00	-78.97	1523	9	1968-2014
M19	Compud	-2.34	-78.94	2402	8	1968-2014
M20	Palmira INAMHI	-2.06	-78.74	3180	4	1968-1991
M21	Achupallas-Chimborazo	-2.28	-78,77	3178	1	1968-2014
M22	Chimbo Pj Pangor	-1.94	-79.00	1452	10	1968-2014
M23	Alausi	-2.20	-78.85	2267	12	1968-2014
M24	Cañi-limbe	-1.77	-78.99	2800	6	1969-2014
M25	Guasuntos	-2.23	-78.81	2438	2	1975-2014
M26	Pangor-J.de Velasco	-1.83	-78.88	3109	11	1970-2014
M27	Colimes de Pajan	-1.58	-80.51	200	2	1970-2014
M28	Vinces INAMHI	-1.56	-79.77	14	8	1968-2014
M29	La Capilla INAMHI	-1,70	-80,00	7	5	1968-2014
M30	Palmeras Unidas (Palmar)	-0.26	-79.60	460	10	1987-2012



Figure 2. Methodological scheme for the regionalization, aggressiveness and concentration of the rain time series.

2.3.1 Method of regional vector

MVR was used to evaluate the quality and estimation of the missing data. This method is oriented to the criticism, homogenization and completion-extension of the precipitation data (Hiez, 1977; Brunet-Moret, 1979). The MVR is based on the creation of a station "average species" type "Vector". This concept refers to the calculation of a weighted average rainfall anomalies for each season, overcoming the effects of seasons with extreme and low rainfall values. Then, there are Z_i annual interposition techniques and P_j 's rainfall, which are extended by the least squares technique. This could be achieved by minimizing the sum of the following equation (Espinoza Villar et al., 2009).

$$\sum_{i=1}^N \sum_{j=1}^M \left(\frac{P_{ij}}{P_j} - Z_i \right) \quad (1)$$

Where i is the year index, j the station index, N the number of years and M the number of stations. P_{ij} represents annual rainfall in the station j , year i ; P_j is the extended average rainy period of N years; and finally, Z_i is the regional rainfall index of the year i . The full set of Z_i values throughout the period is known as the annual vector of regional rainfall indices, and by being an iterative process, this method allows to calculate the vector of each of the vector of the predefined regions, then it provides a comparison of year-on-year variability of stations -vector, to finally discard those that are not consistent with the regional vector (VR). This process is repeated as much as necessary and was performed using the HYDRACCESS software (Vauchel, 2005).

2.3.2 Regionalization

This study used the k-means method, widely employed to regionalize homogeneous areas of precipitation (Golian et al., 2010; Gómez-Latorre, 2015; Shahana Shirin and Thomas, 2016; Rau et al., 2017). K-means is a grouping algorithm, the most commonly used to identify homogeneous groups of objects called clusters. The data within a cluster shares many features but is very different from the data that does not belong to that cluster (Yashwant and Sananse, 2015). The data in this study are summarized in a 30-row matrix for weather stations and 6 columns with information such as: station name, altitude, latitude, longitude and cumulative precipitation. A key part of the k-means application is to define an optimal number of groups, which can be done by estimating the silhouette coefficient (S) for each number of groups, the S coefficient has the advantage that it only considers the current partition and does not depend on the grouping algorithm, its value is obtained by Equation 2 (Rousseeuw, 1987):

$$S_{(i)} = \frac{b_i - a_i}{\max[a_{(i)}, b_{(i)}]} \quad (2)$$

Where $a_{(i)}$ corresponds to the average similarity between object i and other objects in the same group, and $b_{(i)}$ is the average similarity between object i and k-cluster members. The S coefficient varies between -1 and +1; the partition will be better when it gets closer +1, a negative value means that there is no good correspondence between the members of the group, a value of zero means that the object could belong to any group (Kaufman and Rousseeuw, 2005). Also, the homogenization of precipitation was performed for extreme events such as El Niño from 1997-1998, considering the above methodology.

The interpolation of annual precipitation data was performed using a geostatistical approach, co-kriging method, which is a multivariate version of the kriging technique (Goovaerts, 1998), considering two variables (altitude and cumulative precipitation) transformed logarithmically due to the bias and the wide numerical range of precipitation values. This method was used for the interpolation and delimitation of precipitation zones (Rau et al., 2017) and for mapping the spatial distribution of indices.

2.3.3 Climatic aggressiveness analysis and concentration of precipitations

Climate aggressiveness was analyzed by interpreting the Fournier Index (FI) and Modified Fournier Index (MFI). Fournier (1960) proposes a climate aggressiveness index or IF, which has a high correlation with the amount of sediments carried by runoff. The IF estimates the erosive characteristics (aggressiveness) based on the rainiest month of each year within a given time period, and for the calculation of the IF the following expression (3) was used. Where FI: Fournier index for the year j , $p_{\text{máx}}$: average precipitation relative to the wettest month (mm) and P : Average annual precipitation (mm).

$$IF_j = \frac{p_{\text{máx}_j}^2}{P} \quad (3)$$

However, it is necessary to consider areas that have more than a monthly maximum or areas where rainfall values have high values due to seasonality (Jordán and Bellinfante, 2000). To correct these errors, a modification of the original FI was proposed using the accumulated precipitation, called MFI (Arnoldus, 1978). This index considers the rain of the twelve months and not only that of the wettest month, its calculation relates the monthly rainfall with those Equation (4). Where: MFI_j : rainfall aggressiveness index, for year j , p_{ij} : monthly precipitation of the month i (mm) of the year j and P_m : average annual precipitation.

$$MFI_j = \frac{\sum_{i=1}^{12} (p_{ij})^2}{P_m} \quad (4)$$

The seasonality of precipitation was estimated by the Precipitation Concentration Index (PCI) proposed by Oliver (1980), being a distribution indicator of temporal precipitation and used as an estimator of the extreme behavior of the precipitation (Sarricolea et al., 2014). It has traditionally been applied on an annual scale and it describes whether annual precipitation is temporarily concentrated in a single month or distributed evenly throughout the year. The PCI was calculated on an annual scale from the following Equation:

$$PCI_j = 100 \frac{\sum_{i=1}^{12} p_{ij}^2}{P_j^2} \quad (5)$$

The PCI was also analyzed on a seasonal scale considering the periods of increased precipitation (December-May) and lower precipitation (June-November), according to Equation (6):

$$PCI_{\text{seasonal}} = 1000 \frac{\sum_{i=1}^6 P_{ij}^2}{(\sum_{i=1}^6 P_{ij})^2} \quad (6)$$

Where PCI_j : annual rainfall concentration index (%), for year j ; PCI_{estac} : seasonal concentration index (%); p_{ij} : precipitation of month i in year j ; P_j : annual precipitation of the year j . The main difference between these indices is the ranges of rank values (Table 2).

Table 2. Indexes that determine aggressiveness and concentration of precipitation

Index	Classification	
Fournier Index (FI)	<50	Very low
	50-100	low
	100-150	Moderate
	150-200	High
	>200	Very high
Mofidified Fournier Index (MFI)	<100	Very low
	100-200	Low
	200-300	Moderate
	300-400	High
	>400	Very high
Precipitation concentration index (PCI)	8,3 %~10 %	Uniform
	10 %~15 %	Partly seasonal
	15 %~20 %	Seasonal
	20 %~50 %	Strongly seasonal
	50 %~100 %	Irregular

The classification of indices is performed based on (Fournier, 1960; Arnoldus, 1978) and (Oliver, 1980). The influence of climate change on the seasonal pattern of precipitation concentration was determined by Mann-Kendall’s nonparametric statistical test (MK), at three levels of significance (90 %, 95 % y 99 %). MK analysis was performed using TREND software (<https://toolkit.ewater.org.au/trend>). The MK test verifies the existence of positive/negative changes in a series of data, against a zero hypothesis of non-trends and where the data are random and independent (Mann, 1945; Kendall, 1975). MK trend analysis is a robust test when the data differ from "normality" and less sensitive to outliers (Lanzante, 1996). MK analysis has been widely used for the detection analysis of meteorological and hydrological trends (Kumar et al., 2009; Gocic and Trajkovic, 2013; Hermida et al., 2015; Zeleňáková et al., 2016; Güçlü, 2018; Sarricolea et al., 2019).

3 Results and discussion

3.1 Homogenous regions

The optimal value for cluster numbers was determined by the overall average value of S and the number of negative S for each cluster group that varies from 2 to 10 (Table 3). The maximum value of S was obtained for cluster group 2 (0.51) and with a lower number of negative silhouette (1); it is the only group that is considered to be a reasonable structure, because its value of S is greater than 0.50 (Kononenko and Kukar, 2007). Internally cluster group 2 has a strong clustering structure (S=0.66) while cluster 1 reached a lower value, with a negative S (Figure 3b). This indicates that in cluster 1, grouping centers can be found, although there is considerable ‘noise’. Cluster groups for extreme events such as El Niño 97-98 presented similar results (Table 3).

The spatial distributions of K-means (2) show an array of stations according to topographic variation and length (Figure 3). The cluster of two groups divides the CRG into two homogeneous regions of precipitation: lower and middle (red triangles) and upper part (black circles). The two regions are well defined, taking into account the rain interpolation map, as shown in Figure 3a.

Region One (R1) is located on the slopes of the western Andes mountain range and the great plains of the Ecuadorian coast (78,9° a 80,59° O) (Figure 4a). The altitude varies between 3 to 2500 masl, occupying 85,2% of the CRG area. The regime is unimodal, the rainy season runs from December to May (Figure 4b) and concentrates 89% of the accumulated annual rain (Cadier et al., 1996; Rossel and Cadier, 2009; Fries et al., 2014) and a dry season (June-November) (Hastenrath, 1997). The precipitation range ranges from 850 to 3500 mm per year and a year-on-year CV of 0.38 (Figure 4a). The rain in this region is convection type and the distribution of dry and

rainy season is due to the north-south movement of the Intertropical Convergence Zone (ZCIT) (Rollenbeck and Bendix, 2011).

Region two (R2) is located in the western range of the Andes, the altitude is higher than 1500 masl and less than 4000 masl. Rainfall totals (450 to 1500mm year-1) and year-on-year CV (0.34) were relatively low compared to R1 (Figure 4a). The precipitation distribution has a bimodal trend: the first peak occurs from January to May, followed from October to December, and the period May to August has the lowest average monthly precipitation (Figure 4c). The amount of rain that falls in this area is due to the influence of orographic rain and convection (Rollenbeck and Bendix, 2011). Precipitation formation is complex in the mountains due to the interaction between moisture transport, differential surface heating, synoptic wind field and local mountain breeze system (Daly et al., 2007; Foresti and Pozdnoukhov, 2012).

Table 3. Results of the MK analysis for the number of cluster groups.

Cluster group	2	3	4	5	6	7	8	9	10
Average silhouette	0.51	0.46	0.35	0.31	0.34	0.30	0.34	0.27	0.23
Number of negative silhouette	1	3	3	3	2	3	3	4	6
General average of extreme silhouette_events	0.52	0.40	0.26	0.29	0.29	0.26	0.26	0.26	0.26
Number of extreme negative silhouette_events	0	3	4	5	6	5	4	5	5

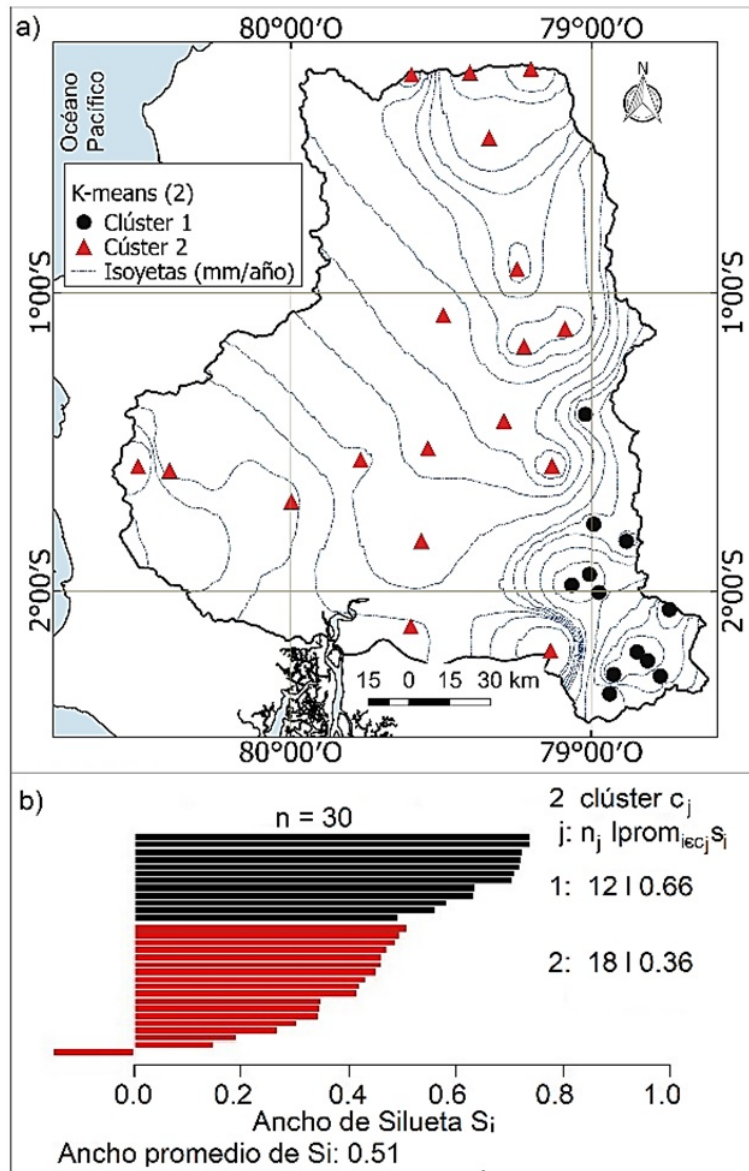


Figure 3. Spatial distribution of the cluster group (2) obtained with the k-means process and its silhouette value.

Two annual precipitation patterns can be identified within the study area: in R1, a well-differentiated annual cycle was found between periods of avenues and styling, characterized by peaks for the years 72-73; 75-76; 91-92; and extreme events for 82-83 and 97-98 (Figure 4d). Extreme rainfall in Ecuador is associated with El Niño events that caused severe flooding, economic losses and disease (Bendix and Bendix, 2006). In R1, the influence of El

Niño is strongly linked to annual rainfall surpluses (Rossel et al., 1998). R2 has a weak seasonality, which is consistent with the estimated average variation coefficient (0.34), where a decrease in average annual precipitation is shown over most seasons compared to R1. Extreme events (82-83 and 97-98) are also observed in the R2 region, because the influence of El Niño in this area is variable (Cadier et al., 1996; Rossel et al., 1998).

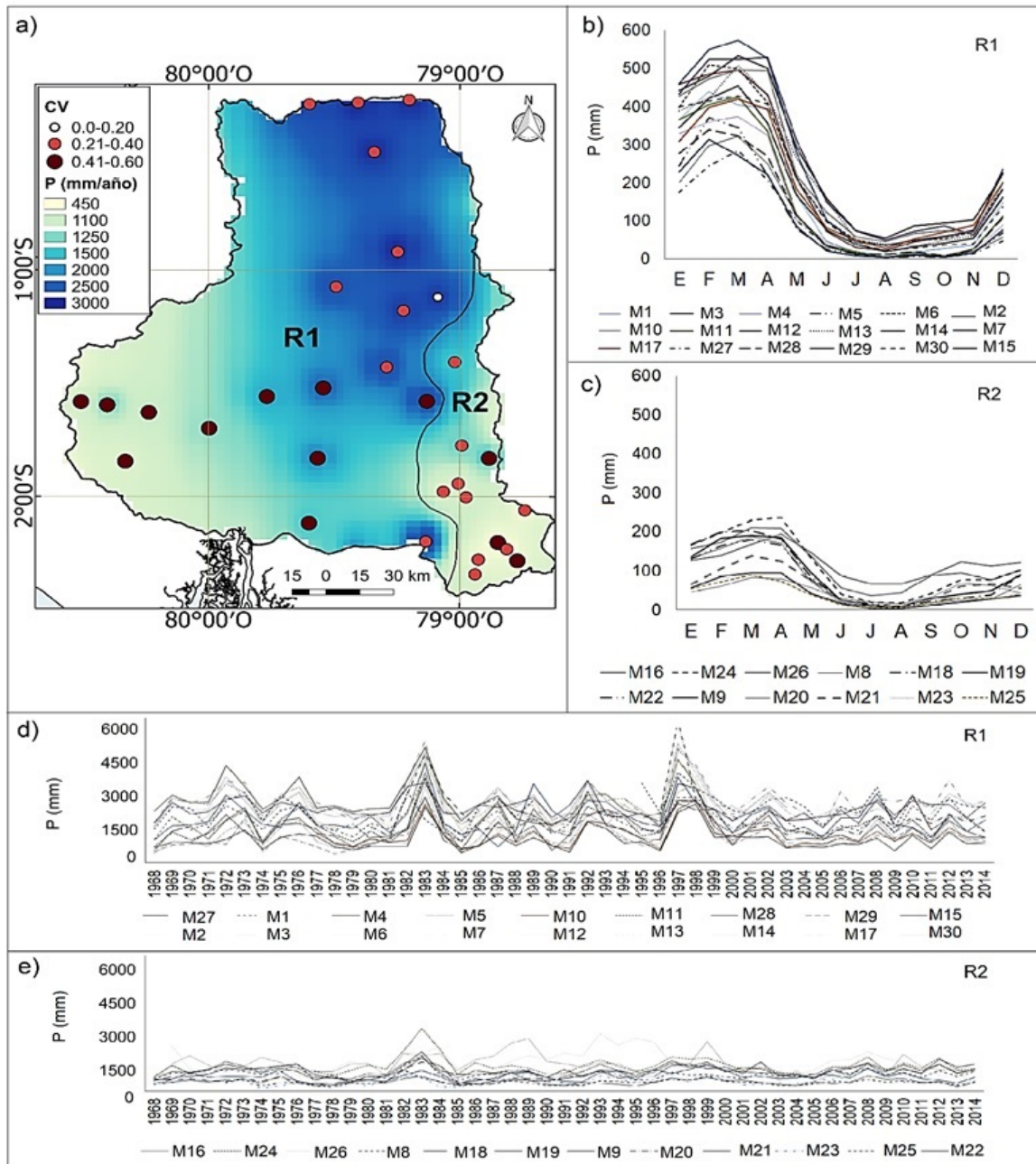


Figure 4. Spatial distribution of the two regions (R1-R2) of homogeneous rain after the regionalization process by k-means. a) Year-on-year variation coefficient (CV) range for the 30 rainfall stations. b) and c) Monthly precipitation regime of R1 and R2. (d) and (e) Annual precipitation distribution (1968–2014) for regions R1 and R2.

3.2 Climatic aggressiveness

In region R1, 45% of the seasons had annual average of FI values greater than 150; this suggests the occurrence of very high erosion rain (Figure 5a). The FI for R2 shows that 50% of the annual average values are less than 50 and remaining values were greater than 50 and less than 100,

considered as very low and low erosion rain, respectively (Figure 5a). Results from MFI suggest a spatial pattern similar to FI (Figure 5b). In fact, in the R1 region, values greater than 300 are values associated with high erosion. While the R2 region has values of approximately 100, indicating low or very low levels of erosion. The difference

in estimated rates for regions R1 and R2 may be associated with the spatial distribution of average annual rainfall (Figure 4a), suggesting a high influence on the seasonality of rainfall in both regions (Figure 4 d-e). Also, the seasonality of the basin is corroborated by the results of the PCI (Figure 5c), as these reach values around 20%, which proposes a predominantly seasonal and strong seasonal clas-

sification. In addition, in the R1 region, the MFI manages to identify eight very high erosion seasons, this may be because the MFI considers the rain of all twelve months and not only that of the rainiest month of the year. Therefore, this methodology might be more appropriate to characterize the severity of the rains in the area under study (Castelan-Vega et al., 2015).

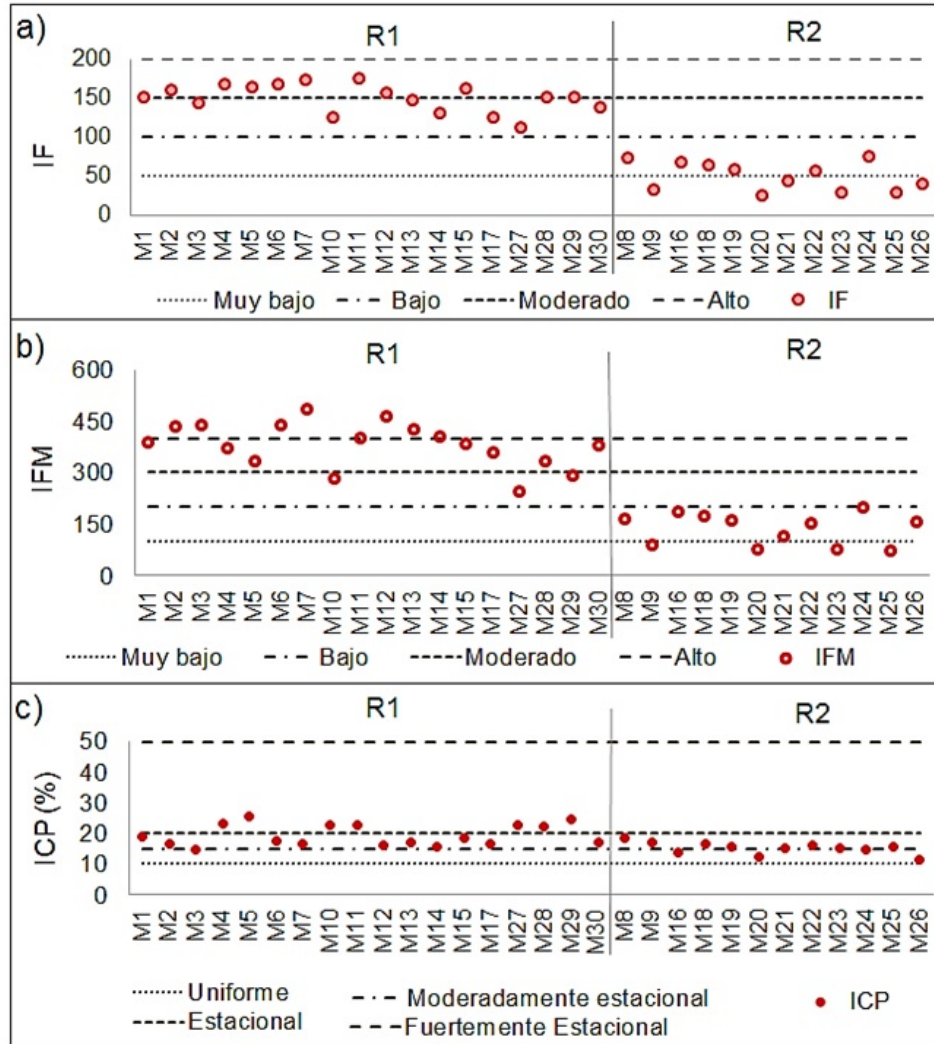


Figure 5. Aggressiveness rates: a) Fournier index (FI), b) Modified Fournier index (MFI) and c) annual mean precipitation concentration (PCI) of 30 stations in the study area.

It is important to mention that the aggressiveness results in region R2 are in agreement with the region with the highest annual precipitation, which has a good correlation and level of significance between the average annual precipitation pattern (mm) with the FI ($r = 0,77, p < 0,01$) and MFI ($r = 0,93, p < 0,01$) (Figure 6 d-e), which confirms that a higher annual accumulation (mm) would

correspond to greater aggressiveness (Besteiro and Delgado, 2011) in areas where annual precipitation is greater than 900 mm (Jordán and Bellinfante, 2000; Rey et al., 2012). Also, a decrease in FI was observed with altitude ($r = 0,85, p < 0,01$), but not so for the MFI. No correlation was found between spatial patterns of climatic aggression for latitude and longitude.

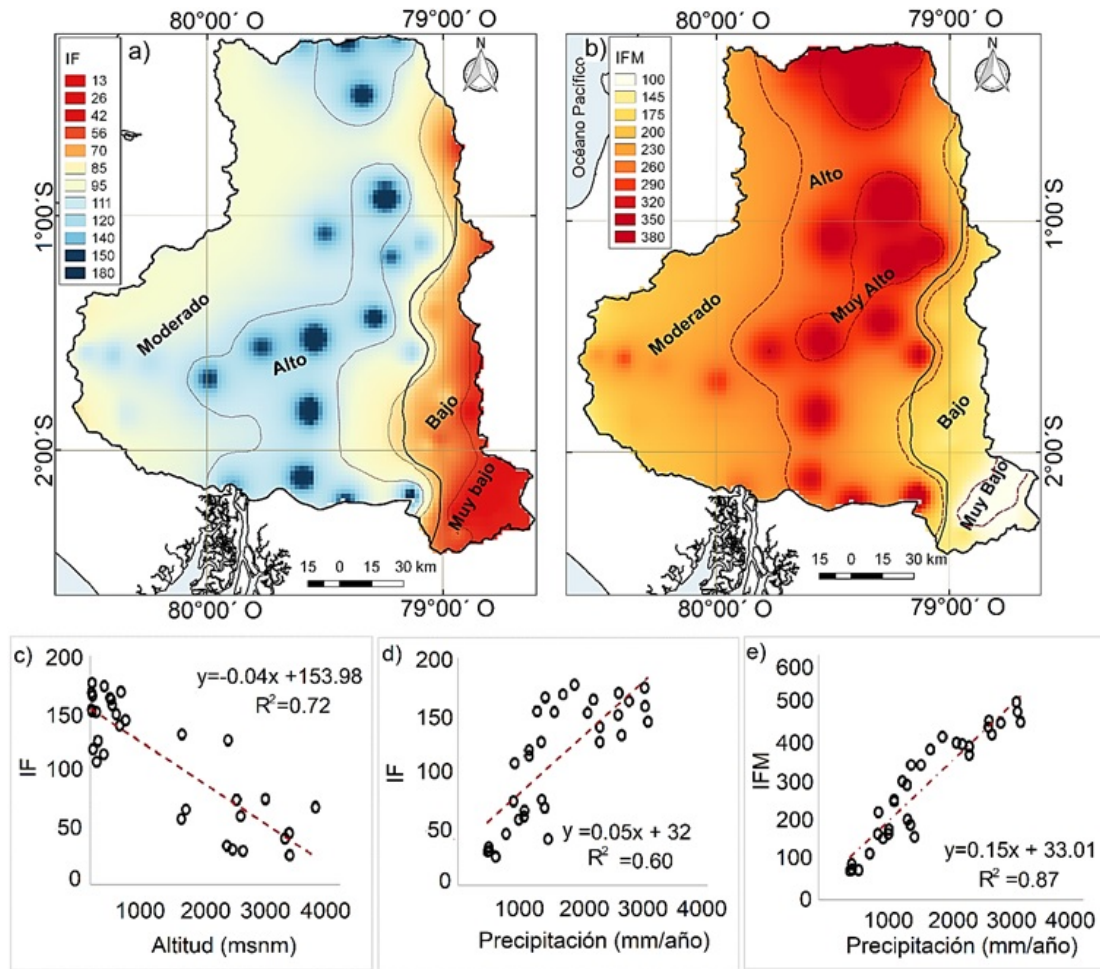


Figure 6. Spatial distribution: a) and b) Annual average aggressiveness (FI, MFI) for the period 1968-2014. Correlation: c) FI with altitude, d) and e) FI and MFI with cumulative precipitation.

3.3 Concentration of precipitations

The historical average annual concentration observed in R1 was distributed seasonally with values ranging from 15–19%, followed by a strongly seasonal distribution (Figure 5c), i.e., precipitation is concentrated within a few months of the year. In region R2, the PCI registers values

higher than 11 and lower than 18%; nine seasons show a seasonal distribution and three moderately seasonal distributions throughout the year (Figure 5c). The historical average annual concentration observed in high mountain regions was predominantly a seasonal and moderately seasonal concentration, these results are consistent with Valdés-Pineda et al. (2016).

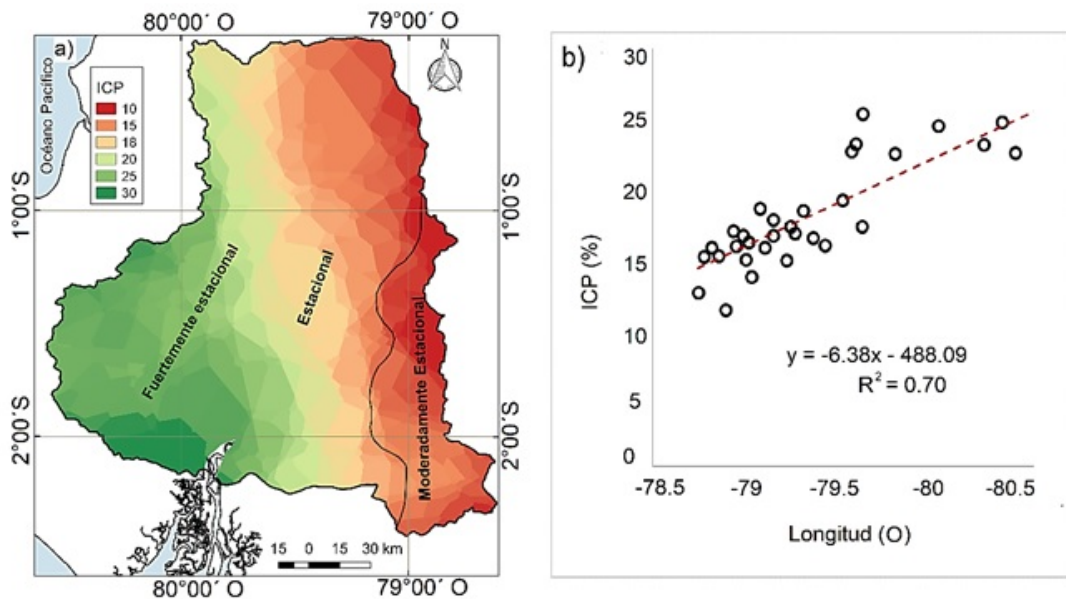


Figure 7. Spatial distribution: a) Annual average rainfall concentration (PCI) for the period 1968-2014 and b) Correlation of the PCI with the length.

The high mountain regions have a rain concentration between seasonal and moderately seasonal, and the central region between strongly seasonal and seasonal (Figure 7a). This suggests a strong association with the length ($r=0.83$, $p<0.01$) (Figure 7b). Along the longitudinal gradient, seasonality increases, leading to a more uniform concentration of annual precipitation. Changes in the PCI are complex, possibly related to global atmospheric characteristics and local and synoptic factors affecting precipitation. However, no correlation was found between PCI with latitude and average annual precipitation, suggesting that the years with the highest annual rainfall are not related to the precipitation concentration. These findings explain why R2 can be strongly affected by seasonal rain during the avenue period, where precipitation that is concentrated in a small number of months is relevant for the occurrence of soil erosion in the upper part, causing sedimentation in the urban area located in the lower part of the CRG.

To analyze changes in seasonal monthly rainfall concentration, the seasonal PCI series (period of highest and lowest precipitation) between 1968 and 2014 was esti-

ated for regions R1 and R2 (Figure 8). Percentages of concentration values around 50% suggests irregularity of precipitation, i.e., a high amount of rain can precipitate in a small number of months, which is associated with flood events; on the other hand, a very low amount of precipitation may be falling in a greater number of months, causing periods of drought that can affect the rain-fed land. This irregularity of monthly rainfall is detected in some years in the dry period of the R1 region (Figure 8). This could affect rain-fed agriculture in the western region of the basin (≈ 1600 masl). Seasonal PCI results ($\approx 20\%$) during the rainy period in R1 and R2 show no significant temporal changes and suggest marked seasonality.

The results of MK's trend analysis identified positive annual trends of the PCI_{estac} only for the dry season (June-November) and negative trends for both periods: dry and rainy. However, in most seasons it does not show a significant trend (Figure 9 a and b). Negative PCI_{estac} trends are concentrated for R1 and R2 in the northern and southeastern part of the CRG.

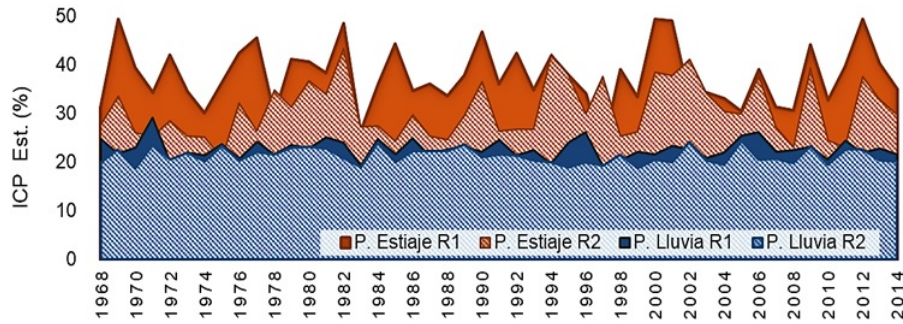


Figure 8. Annual series of seasonal precipitation concentration index (PCI_{estac}) for the period ($P.$) of the section (June to November) and rain (December-May), 1968-2014 for R1 and R2.

For the period of heavy rainfall (December-May), only two seasons show negative trend in R1 and R2, with significance levels of 90% and 99%, respectively (Figure 8a). In the dry period, two stations show significant negative trend at 90 and 95% in the southern region of R1. Also, only one station located in high mountain region re-

gisters positive trend (Figure 8b). In general, the positive or negative trends identified in R1 and R2 indicate changes associated with irregularity of monthly rainfall in the temporal distribution of the concentration; however, this irregularity is identified in very few seasons.

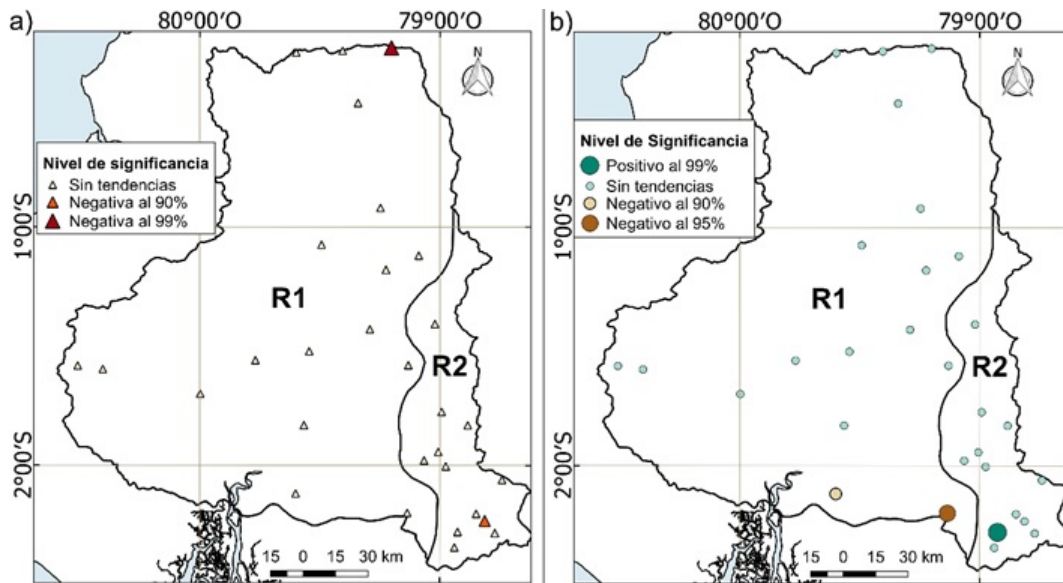


Figure 9. Seasonal distribution of PCI trends (1968–2014) in the Guayas River basin for different significance level ranges: (a) December - May, b) June - November.

4 Conclusions

The study of the aggressiveness of rainfall for the Basin of the Guayas-Ecuador River allowed to homogenize areas of precipitation, characterize the variability of rains in the period 1968 – 2014 and their potential erosive impact. The results suggest two regions 1) west of the basin in the

coastal region up to 2500 masl and 2) east of the basin in the high mountain region between 1500 and 4000 masl. The basin was assessed annually using the Fournier Index (FI), Modified Fournier Index (MFI) and precipitation concentration index (PCI). These findings from IF and MFI indicate that the Guayas River basin in the coastal area is classified as a region of high to very high aggres-

sion in the coastal region, while the high mountain region is classified as low or very low erosion.

Areas of high agricultural activity located in the coastal region have greater erosive potential of rain compared to the high mountain region. The spatial distribution of precipitation concentration increases from east to west, showing moderate to strong seasonality levels. The results using the aggressiveness and concentration of precipitation rates allowed to assess qualitatively the possible impact of rain on the ground and identify aggressiveness patterns with precipitation accumulation and concentration of precipitation associated with the length. This may be associated with seasonal moisture flows from the Equatorial Amazon to the Andes (Espinoza Villar et al., 2009). These results also indicate that the monthly rainfall concentration does not have predominant changes or trends between 1968 and 2014. However, it is recommended to analyze the daily rainfall concentration in equatorial regions, as large percentages of seasonal or annual rain can precipitate in a few days.

References

- Angulo-Martínez, M., López-Vicente, M., Vicente-Serrano, S., and Beguería, S. (2009). Mapping rainfall erosivity at a regional scale, a comparison of interpolation methods in the Ebro basin (NE Spain). *Hydrol. Earth Syst. Sci.*, 13(10):1907–1920. Online: <https://bit.ly/33ucq9c>.
- Arnoldus, H. (1978). *Assessment of erosion*, chapter An approximation of the rainfall factor in the Universal Soil Loss Equation. John Wiley and Sons, Inc., Chichester, England.
- Ballari, D., Giraldo, R., Campozano, L., and Samaniego, E. (2018). Spatial functional data analysis for regionalizing precipitation seasonality and intensity in a sparsely monitored region: Unveiling the spatio-temporal dependencies of precipitation in Ecuador. *International Journal of Climatology*, 38:3337–3354. Online: <https://doi.org/10.1002/joc.5504>.
- Barrera-Crespo, P., Mosselman, E., Giardino, A., Becker, A., Ottevanger, W., Nabi, M., and Arias Hidalgo, M. (2018). Sediment budget analysis of the Guayas river using a process-based model. *Hydrol. Earth Syst. Sci.*, Discuss:1–21. Online: <https://doi.org/10.5194/hess--2018--467>.
- Bendix, A. and Bendix, J. (2006). Heavy rainfall episodes in Ecuador during El Niño events and associated regional atmospheric circulation and SST patterns. *Adv. Geosci.*, 6:43–49. Online: <https://bit.ly/2H3ejjB>.
- Besteiro, S. and Delgado, M. (2011). Evaluación de la agresividad de las precipitaciones en la cuenca del arroyo el pescado, provincia de Buenos Aires (Argentina). *Revista de la Facultad de Agronomía, La Plata*, 110:82–90. Online: <https://bit.ly/2MJ7Fnj>.
- Brunet-Moret, Y. (1979). Homogénéisation des précipitations. *Cahiers ORSTOM. Serie Hydrologie.*, 16(3-4):147–170. Online: <https://bit.ly/2Lfg7Yg>.
- Buckalew, J., Scott, L., James, M., and Reed, P. (1998). Water resources assessment of Ecuador. Technical report, US Army Corps of Engineers (USACE).
- Cadier, E., Rossel, F., Sémiand, H., and Gomez, G. (1996). Las inundaciones en la zona costera ecuatoriana: mecanismos responsables, obras de protección existentes y previstas. Technical report, INESEQ 28.
- Castelan-Vega, R., Tamariz Flores, V., Linares Fleites, G., and Cruz Montalvo, A. (2015). Agresividad de las precipitaciones en la subcuenca del río San Marcos, Puebla, México. *Investigaciones Geográficas*, 83:Online: <https://doi.org/10.14350/rig.33480>.
- Corporación Andina de Fomento (1998). (1998) el fenómeno El Niño 1997-1998. In *Memorias, Retos y Soluciones*, volume IV, pages 72–73, Ecuador.
- Daly, C., Smith, J., and Smith, J.I., M. R. (2007). High-resolution spatial modeling of daily weather elements for a catchment in the Oregon Cascade mountains, United States. *Journal of Applied Meteorology and Climatology*, 46:1565–1586. Online: <https://doi.org/10.1175/JAM2548.1>.
- De Luis, M., González-Hidalgo, J., Brunetti, M., and Longares, L. (2011). Precipitation concentration changes in Spain 1946–2005. *Natural Hazards and Earth System Science*, 11:1259–1265. Online: <https://doi.org/10.5194/nhess--11--1259--2011>.
- Egas, R. (1985). Ecuador, inundaciones 1982 – 1983 en la cuenca baja del Guayas: Procesos de organización de los campesinos para hacer frente al desastre. In J. Haddoy, e. a., editor, *Desastres Naturales y Sociedad en América Latina*. Grupo Editora Latinoamericana.
- Espinoza Villar, J., Ronchail, J., Guyot, J., Cochonneau, G., Naziano, F., Lavado, W., De Oliveira, E., Pomboza, R., and Vauchel, P. (2009). Spatio-temporal rainfall variability in the Amazon basin countries (Brazil, Peru, Bolivia, Colombia, and Ecuador). *International Journal of Climatology*, 29(11):1574–1594. Online: <https://doi.org/10.1002/joc.1791>.
- Foresti, L. and Pozdnoukhov, A. (2012). Exploration of alpine orographic precipitation patterns with radar image processing and clustering techniques: Exploration

- of alpine orographic precipitation patterns. *Meteorological Applications*, 19:407–419. Online: <https://doi.org/10.1002/met.272>.
- Fournier, F. (1960). *Climat et erosion; la relation entre l'érosion du sol par l'eau et les précipitations atmosphériques*. Presses universitaires de France, Paris, France. Online: <https://bit.ly/2L0sM2j>, 1 ed edition.
- Fries, A., Rollenbeck, R., Bayer, F., Gonzalez, V., Oñate Valivieso, F., Peters, T., and Bendix, J. (2014). Meteorology and atmospheric physics. *Catchment precipitation processes in the San Francisco valley in southern Ecuador: combined approach using high-resolution radar images and in situ observations*, 126(1-2):13–29. Online: <https://doi.org/10.1007/s00703--014--0335--3>.
- García-Barrón, L., Morales, J., and Sousa, A. (2018). A new methodology for estimating rainfall aggressiveness risk based on daily rainfall records for multi-decennial periods. *Science of The Total Environment*, 615(15):564–571. Online: <https://doi.org/10.1016/j.scitotenv.2017.09.305>.
- Gobierno Provincial del Guayas (2016). Plan provincial de riego y drenaje del guayas. gaceta oficial del gobierno autónomo descentralizado provincial del guayas. año 1. Technical Report 90, Guayaquil.
- Gobierno Provincial del Guayas (2018). Estudio de impacto ambiental del proyecto dragado de la ii fase y disposición de los sedimentos de los alrededores del islote el palmar en la provincia del guayas considerando como sitios de depósito isabel ana, lotización el tejtar, caracoles y terrenos particulares del cantón durán. Technical report.
- Gocic, M. and Trajkovic, S. (2013). Analysis of changes in meteorological variables using mann-kendall and sen's slope estimator statistical tests in serbia. *Global and Planetary Change*, 100:172–182. Online: <https://doi.org/10.1016/j.gloplacha.2012.10.014>.
- Golian, S., Saghafian, B., Sheshangosht, S., and Ghalkhani, H. (2010). Comparison of classification and clustering methods in spatial rainfall pattern recognition at northern iran. *Theoretical and Applied Climatology*, 102:319–329. Online: <https://doi.org/10.1007/s00704--010--0267--x>.
- Goovaerts, P. (1998). Geostatistics for natural resources evaluation. *Geological Magazine*, 135(6):819–842. Online: <https://bit.ly/30Jsxho>.
- Gregori, E., Andrenelli, M., and Zorn, G. (2006). Assessment and classification of climatic aggressiveness with regard to slope instability phenomena connected to hydrological and morphological processes. *Journal of Hydrology*, 329:489–499. Online: <https://doi.org/10.1016/j.jhydrol.2006.03.001>.
- Güçlü, Y. (2018). Multiple Şen-innovative trend analyses and partial mann-kendall test. *Journal of Hydrology*, 566:685–704. Online: <https://doi.org/10.1016/j.jhydrol.2018.09.034>.
- Gómez-Latorre, D. (2015). Regionalización de patrones de precipitación para periodos multianuales secos y húmedos en el altiplano cundiboyacense. page Online: <https://bit.ly/327Z9BO>.
- Hastenrath, S. (1997). Annual cycle of upper air circulation and convective activity over the tropical americas. *Journal of Geophysical Research: Atmospheres*, 102:4267–4274. Online: <https://doi.org/10.1029/96JD03122>.
- Hermida, L., López, L., Merino, A., Berthet, C., García-Ortega, E., Sánchez, J., and Dessens, J. (2015). Hailfall in southwest france: Relationship with precipitation, trends and wavelet analysis. *Atmospheric Research*, 156:174–188. Online: <https://doi.org/10.1016/j.atmosres.2015.01.005>.
- Hernando, D. and Romana, M. (2016). Estimate of the (r) usle rainfall erosivity factor from monthly precipitation data in mainland spain. *J. Iber. Geol.*, 42:113–124. Online: https://doi.org/10.5209/rev_JIGE.2016.v42.n1.49120.
- Hiez, G. (1977). Lhomogénéité des données pluviométriques. *Cahiers ORSTOM. Serie Hydrologie*, 14(2):111–119.
- Jordán, A. and Bellinfante, N. (2000). Cartografía de la erosividad de la lluvia estimada a partir de datos pluviométricos mensuales en el campo de gibraltar (cádiz). *Edafología*, 7(3):83–92.
- Kaufman, L. and Rousseeuw, P. (2005). *Finding groups in data: an introduction to cluster analysis*. Wiley series in probability and mathematical statistics. Wiley, Hoboken, N.J.
- Kendall, M. (1975). *Rank Correlation Methods*. Griffin, London, UK.
- Kinnell, P. (2010). Event soil loss, runoff and the universal soil loss equation family of models: review. *J. Hydrol.*, 385.
- Kononenko, I. and Kukar, M. (2007). *Machine Learning and Data Mining: Introduction to Principles and Algorithms*. Horwood Publishing, Chichester, UK. Online: <https://bit.ly/2L0pL1Q>.
- Kumar, S., Merwade, V., Kam, J., and Thurner, K. (2009). Streamflow trends in indiana: Effects of long term persistence, precipitation and subsurface drains. *Journal of Hydrology*, 374:171–183. Online: <https://doi.org/10.1016/j.jhydrol.2009.06.012>.

- Lanzante, J. (1996). Resistant, robust and non-parametric techniques for the analysis of climate data: Theory and examples, including applications to historical radiosonde station data. *International Journal of Climatology*, 16(11):1197–1226. Online: <https://bit.ly/2OQzqok>.
- Mann, H. (1945). Nonparametric tests against trend. *Econometrica*, 13:245–259. Online: <https://bit.ly/2ZvPQOj>.
- Martín-Fernández, L. and Martínez-Núñez, M. (2011). An empirical approach to estimate soil erosion risk in Spain. *Science of The Total Environment*, 409:3114–3123. Online: <https://doi.org/10.1016/j.scitotenv.2011.05.010>.
- Mondal, A., Khare, D., and Kundu, S. (2016). Change in rainfall erosivity in the past and future due to climate change in the central part of India. *International Soil and Water Conservation Research*, 4(3):186–194. Online: <https://doi.org/10.1016/j.iswcr.2016.08.004>.
- Oliver, J. (1980). Monthly precipitation distribution: a comparative index. *The Professional Geographer*, 32(3):300–309. Online: <https://doi.org/10.1111/j.0033-0124.1980.00300.x>.
- Panagos, P., Ballabio, C., Borrelli, P., Meusburger, K., Klik, A., Rousseva, S., Tadic, M., Michaelides, S., Hrabalíková, M., Olsen, P., Aalto, J., Lakatos, M., Rymaszewicz, A., Dumitrescu, A., Beguería, S., and Alewell, C. (2015). Rainfall erosivity in Europe. *Science of The Total Environment*, 511:801–814. Online: <https://doi.org/10.1016/j.scitotenv.2015.01.008>.
- Parracho, A., Melo-Gonçalves, P., and Rocha, A. (2016). Regionalisation of precipitation for the Iberian Peninsula and climate change. *Physics and Chemistry of the Earth, Parts A/B/C*, 94:146–154. Online: <https://doi.org/10.1016/j.pce.2015.07.004>.
- Prakash, S., Mitra, A., Agha Kouchak, A., and Pai, D. (2015). Error characterization of TRMM multi-satellite precipitation analysis (TMPA-3B42) products over India for different seasons. *Journal of Hydrology*, 529:1302–1312. Online: <https://doi.org/10.1016/j.jhydrol.2015.08.062>.
- Rau, P., Bourrel, L., Labat, D., Melo, P., Dewitte, B., Frapart, F., Lavado, W., and Felipe, O. (2017). Regionalization of rainfall over the Peruvian Pacific slope and coast: Regionalization of rainfall (Peruvian coast). *International Journal of Climatology*, 37:143–158. Online: <https://doi.org/10.1002/joc.4693>.
- Rey, J., Rodríguez, M., Cortez, A., Lobo, D., Ovalles, F., and Gabriels, D. (2012). Análisis de la agresividad y concentración de las precipitaciones en Venezuela. IV. Región Los Andes. *BioAgro*, 24:115–120. Online: <https://bit.ly/2MIEaSv>.
- Reynaud, J.-Y., Witt, C., Pazmiño, A., and Gilces, S. (2018). Tide-dominated deltas in active margin basins: Insights from the Guayas estuary, Gulf of Guayaquil, Ecuador. *Marine Geology*, 403:165–178. Online: <https://doi.org/10.1016/j.margeo.2018.06.002>.
- Rollenbeck, R. and Bendix, J. (2011). Rainfall distribution in the Andes of southern Ecuador derived from blending weather radar data and meteorological field observations. *Atmospheric Research*, 99:277–289. Online: <https://doi.org/10.1016/j.atmosres.2010.10.018>.
- Rossel, F., Caddier, E., and G., G. (1996). Las inundaciones en la zona costera ecuatoriana: causas; obras de protección existentes y previstas. *Bull. Inst. fr. études andines*, 25(3):399–420.
- Rossel, F. and Cadier, E. (2009). El Niño and prediction of anomalous monthly rainfalls in Ecuador. *Hydrological Processes*, 23:3253–3260. Online: <https://doi.org/10.1002/hyp.7401>.
- Rossel, F., Mejía, R., Ontaneda, G., Pombosa, R., Roura, J., Goulven, P., and Calvez, R. (1998). Régionalisation de l'influence du El Niño sur les précipitations de l'équateur. *Bull. Inst. fr. études andines*, 27(3):643–654. Online: <https://bit.ly/2zoRFOD>.
- Rousseeuw, P. (1987). Silhouettes: A graphical aid to the interpretation and validation of cluster analysis. *Journal of Computational and Applied Mathematics*, 20:53–65. Online: [https://doi.org/10.1016/0377-0427\(87\)90125-7](https://doi.org/10.1016/0377-0427(87)90125-7).
- Sanchez-Moreno, J., Mannaerts, C., and Jetten, V. (2014). Rainfall erosivity mapping for Santiago Island, Cape Verde. *Geoderma*, 217:74–82. Online: <https://doi.org/10.1016/j.geoderma.2013.10.026>.
- Sarricolea, P., Araya, C., and Salazar, P. (2014). Concentración de las precipitaciones en Chile central y su relación con los patrones de variabilidad de baja frecuencia, período 1965–2010, pages 305–314. Online: <https://bit.ly/30J8DmS>.
- Sarricolea, P., Meseguer-Ruiz, S., Serrano-Notivol, R., Soto, M., and Martín-Vide, J. (2019). Trends of daily precipitation concentration in central-southern Chile. *Atmospheric Research*, 215:85–98. Online: <https://doi.org/10.1016/j.atmosres.2018.09.005>.
- Shahana Shirin, A. and Thomas, R. (2016). Regionalization of rainfall in Kerala state. *Procedia Technology*, 24:15–22. Online: <https://doi.org/10.1016/j.protcy.2016.05.004>.
- Soledispa, B. (2002). Estudio de los sedimentos del sector donde convergen los ríos Daule y Babahoyo, y las posibles causas que están formando un nuevo islote en ese sector. *Acta Oceanográfica del Pacífico*, 11(1):185–201.

- Terranova, O., Antronico, L., Coscarelli, R., and Iaquin-ta, P. (2009). Soil erosion risk scenarios in the medi-terranean environment using rusle and gis: an appli-cation model for calabria (southern italy). *Geomorp-hology*, 112:228–245. Online: <https://doi.org/10.1016/j.geomorph.2009.06.009>.
- Thi Nguyen, T., Boets, P., Lock, K., Damanik Ambari-ta, M., Forio, M., Sasha, P., Dominguez-Granda, L., Thi Hoang, T., Everaert, G., and Goethals, P. (2015). Hab-itat suitability of the invasive water hyacinth and its relation to water quality and macroinvertebrate diver-sity in a tropical reservoir. *Limnologica*, 52:67–74. Onli-ne:<https://doi.org/10.1016/j.limno.2015.03.006>.
- Twilley, R. R., Cárdenas, W., Rivera-Monroy, V. H., Espi-noza, J., Suescum, R., Armijos, M. M., and Solórzano, L. (2001). *The Gulf of Guayaquil and the Guayas River Estuary, Ecuador*, pages 245–263. Online: https://doi.org/10.1007/978--3--662--04482--7_18. Springer Ber-lin Heidelberg, Berlin, Heidelberg.
- Valdés-Pineda, R., Pizarro, R., Valdés, J., Carrasco, J., García-Chevesich, P., and Olivares, C. (2016). Spatio-temporal trends of precipitation, its aggres-siveness and concentration, along the pacific coast of south america (36–49°s). *Hydrological Scien-ces Journal*, 61:2110–2132. Online:<https://doi.org/10.1080/02626667.2015.1085989>.
- Vauchel, P. (2005). Hydraccess: Software for management and processing of hydro-meteorological data software, version 2.1.4. Free download. Online: <https://www.mpl.ird.fr/hybam/utills/hydracces.html>.
- Vrieling, A., Hoedjes, J. C. B., and van der Velde, M. (2014). Towards large-scale monitoring of soil erosion in africa: Accounting for the dynamics of rainfall ero-sivity. *Global and Planetary Change*, 115:33–43. Onli-ne:<https://doi.org/10.1016/j.gloplacha.2014.01.009>.
- Yashwant, S. and Sananse, S. (2015). Comparisons of different methods of cluster analysis with applica-tion to rainfall data. *International Journal of Inno-vative Research in Science, Engineering and Technology*, 4(11):10861–10872. online: <https://bit.ly/347RXre>.
- Zeleňáková, M., Purcz, P., Poórová, Z., Alkhalaf, I., Hla-vatá, H., and Portela, M. (2016). Monthly trends of pre-cipitation in gauging stations in slovakia. *Procedia Engi-neering*, 162:106–111. Online: <https://doi.org/10.1016/j.proeng.2016.11.023>.
- Zubieta, R., Saavedra, M., Espinoza, J., Ronchail, J., Sul-ca, J., Drapeau, G., and Martin-Vide, J. (2019). As-sessing precipitation concentra-tion in the amazon ba-sin from different satellite-based datasets. *Int. J. Cli-matol*, 39:3171– 3187. Online: <https://doi.org/10.1002/joc.6009>.
- Zubieta, R., Saavedra, M., Silva, Y., and Giráldez, L. (2016). Spatial analysis and temporal trends of daily precipitation concentration in the mantaro river basin: central andes of peru. *Stochastic Environmental Research and Risk Assessment*, pages 1–14. Online: <https://doi.org/10.1007/s00477--016--1235--5>.